ELSEVIER

Journal of Alloys and Compounds 456 (2008) 16–26

Journal of ALLOYS AND COMPOUNDS

www.elsevier.com/locate/jallcom

Comprehensive analysis of crystal field parameter datasets for transition ions at low symmetry sites and extracting structural information—Application to Pr^{4+} in $BaPrO_3$

Czesław Rudowicz *, Paweł Gnutek

Institute of Physics, Szczecin University of Technology, Al. Piastów 17, 70-310 Szczecin, Poland

Received 17 January 2007; received in revised form 8 February 2007; accepted 9 February 2007
Available online 21 February 2007

Abstract

Our recent literature survey has revealed several crystal field parameter (CFP) datasets for rare-earth ions at orthorhombic, monoclinic, and triclinic symmetry sites in various hosts. Often CFP datasets are not directly comparable, even for the same ion-host system, whereas the low symmetry effects observed may be either actual or apparent. Careful considerations are required to distinguish the nature of the low symmetry effects and extract useful structural information inherent in the low symmetry CFPs. For this purpose, we propose a comprehensive approach comprising three methods. First method consists in finding the principal values of the second-rank CFPs and the orientation of their principal axis system w.r.t. the original or crystallographic axis system. Second method consists in extending the cubic/axial pseudosymmetry axes method to lower symmetry cases. Third method consists in considering for quantitative comparison of CFP datasets of the closeness factors C_p and the norms ratios $R_p = N_A/N_B$ for the respective H_{CF} terms: $p = k = 2$, 4, and 6, and the global (p = gl) ones. Usefulness of the various physically equivalent CFP datasets generated by the first and second method as initial sets for the multiple correlated fitting technique is also discussed. This study benefits from cross-fertilization between the spin Hamiltonian theory used in the EMR area and the CF theory, since these methods have been used before in the EMR area. As an application of this approach, for the first time in the CF theory area, we reanalyze the triclinic-like CFPs and the low symmetry effects involved therein as well as the cubic CFPs for Pr^{4+} in $BaPrO_3$.

PACS: 71.70.Ch crystal and ligand fields; 75.10.Dg crystal-field theory and spin Hamiltonians; 76.30.Kg rare-earth ions and impurities; 02.20.−a group theory

Keywords: Insulators; Crystal structure and symmetry; Crystal and ligand fields; Light absorption and reflection; Electron paramagnetic resonance; Crystal-field Hamiltonian; Ligand-field Hamiltonian; Standardization; Low symmetry effects; Pseudosymmetry axes method; $BaPrO_3$

1. Introduction

The crystal field parameter (CFP) datasets for rare-earth ions at orthorhombic, monoclinic, and triclinic symmetry sites in various hosts, revealed by our recent literature survey, are often disparate and thus not directly comparable even for the same ion-host system. Each symmetry case presents specific intricacies, which are often not realized by experimentalists [1]. Among others, it appears that upon appropriate transformations such datasets may turn out to be either physically equivalent or completely inconsistent. For rare-earth ions at triclinic sites, the symbolic CFPs [1], i.e. those used in the CF Hamiltonian, expressed in their original axis systems include for a given rank $k = 2$, 4, 6, all components, $-k \le q \le +k$, admissible by group theory. Using all 27 symbolic CFPs for fitting the experimental spectra, i.e. the 'complete' C-approach, yields the experimentally fitted CFPs that shall be considered as expressed in an undefined 'nominal' axis system [1]. The C-approach does not utilize fully the information inherent in the CFP datasets. Theoretical calculations of CFPs based on various models, which most commonly employ the crystallographic axis system centered at rare-earth ion, may also yield triclinic-like CFP datasets. However, 'triclinicity' of the model CFPs turns out to be apparent in the cases when (i) the local site symmetry is actually higher than triclinic or (ii) the crystallographic axis system does not coincide with the symmetry-adapted axis system. Careful considerations are required to distinguish the nature of the low symmetry effects and extract useful structural information

* Corresponding author. Tel.: +48 91 449 4286; fax: +48 91 449 4181.
E-mail address: crudowicz@ps.pl (C. Rudowicz).

0925-8388/$ – see front matter © 2007 Elsevier B.V. All rights reserved.
doi:10.1016/j.jallcom.2007.02.088

inherent in the CFPs for the symmetry cases in question. Such considerations are carried out here using as an example the CFP datasets for Pr^{4+} ion in $BaPrO_3$ [2] and utilizing the comprehensive approach comprising three methods described in details in Refs. [3–5]. Preliminary results have been presented at a conference [6].

Preliminary results have been presented at the 6th International Conference on f-elements, 4–9 September 2006, Wrocław, Poland [6]. In this paper we provide the full results of analysis of the triclinic-like crystal field parameter (CFP) [2] dataset as well as the cubic ones obtained by various authors for Pr^{4+} ion in $BaPrO_3$. The triclinic-like CFPs were calculated using the exchange charge model (ECM) by Popova et al. [2]. Our comprehensive approach comprises three recently developed methods: (i) the procedure for diagonalization of the second-rank CFPs [3], (ii) an extension of the cubic/axial pseudosymmetry axes method of Bacquet et al. [4] to lower symmetry cases [5], and (iii) quantitative comparison of CFP datasets and other quantities based on the closeness factors C_p and the norms ratios $R_p = N_A/N_B$ for the respective H_{CF} terms: $p = k = 2, 4, 6$, and the global (p = gl) ones [1,7]. The method (i) provides the principal values of the second-rank CFPs and the orientation of their principal axis systems w.r.t. the original axis system. The method (ii) provides the pseudosymmetry axis systems that best reflect the approximation to a selected higher symmetry case. This is achieved by minimizing an appropriate combination of the CFPs w.r.t. the Euler angles, which define the resulting pseudosymmetry axis system. So obtained CFP sets exhibit the maximal and minimal values of the given higher symmetry CFPs and the out-of-given symmetry ones, respectively. This enables comparison with the experimental CFPs fitted using higher albeit approximated symmetry, e.g. cubic. The method (iii) provides means for quantitative comparison of various sets of N quantities of the same nature, e.g. the CFPs or the energy levels, considered as N-dimensional 'vectors'. Comparison and correlation of various axis systems considered here enable to extract useful structural information inherent in the low symmetry CFP datasets but not hitherto utilized. Our three-method approach and analysis of the respective results may facilitate correlation of the optical spectroscopy data with the structural data obtained from X-ray studies. In Section 2 we discuss thoroughly the aspects bearing on the reliability of the triclinic-like and cubic CFPs for Pr^{4+} ion in $BaPrO_3$ as well as some inconsistencies revealed in Ref. [2]. In Section 3 we apply the three-method approach to analyze the triclinic-like CFPs and consider the nature of the low symmetry effects involved.

2. Crystal field parameters for Pr^{4+} ion in $BaPrO_3$

The first observation of the optical spectrum of Pr^{4+} in $BaPrO_3$ was reported in Ref. [8]. The local site symmetry of the four-fold coordinated Pr^{4+} ions in $BaPrO_3$ (orthorhombic space group *Pbnm*) is considered as C_i due to distortion of the approximated octahedral O_h symmetry [2]. The cubic symmetry was used as a first approximation in the optical spectroscopy studies of Pr^{4+} in $BaPrO_3$ [2,8–11]. The unit cell of $BaPrO_3$ drawn based on the crystallographic data [12] for $T = 300$ K and the definition of the crystallographic axis system ($x||a, y||b, z||c$) as well as the four adjacent Pr–O_6 octahedra obtained from these data indicating the buckling of octahedra were presented in Fig. 1 of Ref. [6]. The $BaPrO_3$ unit cell contains four magnetically inequivalent Pr^{4+} sites at positions given in terms of the units vectors (**a**, **b**, **c**) as (0.5, 0, 0)—Pr1, (0, 0.5, 0)—Pr2, (0.5, 0, 0.5)—Pr3 and (0, 0.5, 0.5)—Pr4. These sites are related by symmetry operations [2].

Based on the ECM [13] and using the crystallographic data [12] for $T = 300$ K, Popova et al. [2] calculated theoretically the CFPs originally defined by the CF Hamiltonian [13]:

$$H_{CF} = B_{pq}\eta_p O_p^q \tag{1}$$

where O_p^q and η_p were termed as "the Stevens operators and the reduced matrix elements" without providing any references for their definitions. In their Table 2 [2] another symbol B_{pk} appears indicating explicitly p as the rank and k as the component. The notation [13,2] in Eq. (1) differs from the well-established notations for the usual and extended Stevens operators [14–18] and the associated CFPs (as well as the zero-field splitting ones) reviewed in Refs. [14,15]. As discussed in Ref. [19], H_{CF} (1) is equivalent to the prevailing [14–17,20] one:

$$H_{CF} = \sum_{k,q} B_k^q O_k^q(\mathbf{J} \text{ or } \mathbf{L}) = \sum_{k,q} A_k^q \left\langle r^k \right\rangle \theta_k O_k^q = \sum_{k,q} C_k^q \theta_k O_k^q \tag{2}$$

where k denotes the rank and q the component, whereas θ_k ($=\eta_p$) $= \alpha, \beta$, and γ for $k = 2, 4$, and 6, respectively, are the Stevens factors [16]. Note that different Stevens factors apply for the excited multiplet $^2F_{7/2}$ than for the ground one $^2F_{5/2}$, whereas the two types of the Stevens factors $\langle J|\theta_k|J\rangle$ and $\langle J|\theta_k|J+1\rangle$ are listed in Ref. [16]. Hence, doubts arise which factors have been actually used in Ref. [2]. Therefore, in order to avoid further confusion, for data presentation below we use the original CFP values of Table 2 in Ref. [2] denoted as B_{kq} (k as the rank and q as the component) without converting them to the CFPs C_k^q defined in Eq. (2).

Under the combined action of the spin-orbit coupling and the octahedral CF, the f^1 configuration splits into three Kramers doublets and two quartets yielding four possible transitions; see, e.g. [2,9,11]. At the lower symmetry CF only the quartets splits, yielding total six transitions, which can be used for fitting the CFPs. Hence, it is impossible to fit all 27 CFPs required for Pr^{4+} ions at triclinic symmetry sites. The ECM [2] employed instead three dimensionless parameters of the model G_k, $k = 2, 4$, and 6, together with the spin-orbit coupling constant λ. The values of these four parameters were obtained by matching the theoretical energy levels with the optical data. The interplay between the spin-orbit coupling and CF is important since adjusting the value of λ affects the resulting values of the CFPs. This is due to the fact that the splitting between the multiplets $^2F_{5/2}$ and $^2F_{7/2}$ by spin-orbit coupling is about 3000 cm^{-1}, i.e. comparable with splitting of $^2F_{5/2}$ by CF of about 2000 cm^{-1}.

Concerning the cubic CFPs determined by various authors for Pr^{4+} in $BaPrO_3$, the following comments are pertinent. Doubts arise concerning the numerical conversion in Ref. [2] of the

cubic CFPs for Pr^{4+} in $BaCeO_3$ [10] used for comparison with their CFPs for Pr^{4+} in $BaPrO_3$. The prevailing cubic H_{CF} form expressed in the tetragonal fourfold axes in the notation of Eq. (2) [14,16]:

$$H_{CF} = C_4^0\beta(O_4^0 + 5O_4^4) + C_6^0\gamma(O_6^0 - 21O_6^4) \quad (3)$$

yields the relations for the cubic CFPs: $C_4^4 = 5C_4^0$ and $C_6^4 = -21C_6^0$. Note that a rotation of the coordinate system by 45° around the z-axis parallel to the four-fold symmetry axis, with the x- and y-axis taken as the two-fold symmetry axis, yields instead of Eq. (3) the form:

$$H_{CF} = C_4^0\beta(O_4^0 - 5O_4^4) + C_6^0\gamma(O_6^0 + 21O_6^4). \quad (4)$$

It appears the authors [2] implicitly use the relations for the cubic CFPs: $C_4^4 = -5C_4^0$ and $C_6^4 = 21C_6^0$, which differ in signs from those in Eq. (3). It is not clear if such rotation has been implicitly implemented in Ref. [2] or the signs of the two cubic CFPs have been changed inadvertently. Note that the sign convention for the two parameters in question is completely arbitrary, since -replacing C_4^4 and C_6^4 by $-C_4^4$ and $-C_6^4$ does not change any predicted energy level. However, it should be kept in mind that this convention applies only for cubic and tetragonal cases. For orthorhombic or lower symmetry case we have to consider other orthorhombic-like parameters C_k^2 and C_k^6, which transform under the 45°/Oz rotation into $-C_k^{-2}$ and $-C_k^{-6}$, respectively. Thus for symmetry lower than cubic or tetragonal, meaningful comparison of all CFPs requires consideration implications of the 45°/Oz rotation also for the orthorhombic and/or lower symmetry CFPs [21]. The signs of the cubic CFPs have structural implications discussed in Section 3. The CFPs in Ref. [10] were expressed in terms of the energy differences: $\Delta = E(\Gamma_5) - E(\Gamma_2) = 1686\,cm^{-1}$ and $\Theta = E(\Gamma_4) - E(\Gamma_5) = 2521\,cm^{-1}$, where Γ_i denote the cubic irreps for the f^1 configuration. Assuming $A_k\langle r^k\rangle = C_k^0$ and using the expressions $7R = \Delta$, $7Q = \Theta$, $C_4^0 = 21(3Q + 2R)/32$, and $C_6^0 = 39(5Q - 4R)/640$ [9], we obtain $C_4^0 = 1025\,cm^{-1}$ and $C_6^0 = 51\,cm^{-1}$. According to the prevailing conventions, these values would yield $C_4^4 = 5125\,cm^{-1}$ and $C_6^4 = -1071\,cm^{-1}$, instead of the values listed in Ref. [2]: $C_4^4 = -5075\,cm^{-1}$ (this value may be misprinted in Ref. [2] for $-5125\,cm^{-1}$) and $C_6^4 = 1071\,cm^{-1}$.

In the neutron scattering study [11] indicates the excited level $\Gamma_8 = (255 \pm 10)\,meV$ ($2056.7 \pm 80.6\,cm^{-1}$), which yields the cubic experimental CFP $V_4 = (119 \pm 4)\,meV$ ($959.8 \pm 32.3\,cm^{-1}$), whereas the CFP V_6 was approximately estimated as the ratio $V_6/V_4 \approx 0.05$. Hence, we obtain: $C_4^0 = V_4 = 959.8$, $C_4^4 = 5V_4 = 4799.0$, $C_6^0 = V_6 = 0.05V_4 = 48.0$, $C_6^4 = -21V_6 = -1007.8$ (cm^{-1}). The magnetic susceptibility study [9] of Pr^{4+} in $BaPrO_3$ provided two sets of the cubic CFPs [$7R$, $7Q$]: (1) [1562, 2881], and (2) [1562, 1267] (cm^{-1}), which yield correspondingly [C_4^0, C_6^0, C_4^4, C_6^4, C_6^0/C_4^0] as: (1) [1103, 71, 5516, 1491, 0.05] and (2) [649, 0.76, 3245, 15.96, 0.001] (cm^{-1}). Set (1) was considered as more reliable, since it yielded better description of the values $|\mu_{eff}| = 0.7(1)\mu_B$, spin-orbit coupling constant $\xi_f = 865\,cm^{-1}$, and the excited level $\Gamma_8 = 2057 \pm 81\,cm^{-1}$ [11]. The set (2) arises from an attempt to fit the experimental magnetic susceptibility data in Fig. 4 in Ref. [9] using the values $\Gamma_8 = 1550\,cm^{-1}$, $7R = 1562\,cm^{-1}$, and $\xi_f = 865\,cm^{-1}$, which yield $7Q = 1267\,cm^{-1}$. The so recalculated values of C_4^0 and the ratio C_6^0/C_4^0 for set (1) correspond better than those for set (2) to the values obtained in Ref. [9]. The authors [9] provide also explicitly the values $C_4^0 = 1100\,cm^{-1}$ and $C_6^0 = 71\,cm^{-1}$, which correspond to their set (1) and agree well with those recalculated by us above based on the cubic CFPs [9]. In view of the disagreement in signs of the cubic CFPs in Ref. [2] and the other literature data [8–11], the cubic, and thus by implication the triclinic-like CFPs [2], should be treated with caution.

3. Analysis of the CFPs for Pr^{4+} ion in $BaPrO_3$

For this study we have developed computer package DPC comprises three modules [6]: (i) module 3DD—for diagonalization of the second-rank CFPs, (ii) module PAM—for extension of the pseudosymmetry axes method to lower symmetry cases that enables finding the pseudosymmetry axis system for the fourth-rank CFPs, and (iii) module CFNR—for calculations of the closeness factors and the norms ratios for quantitative comparison of CFP datasets and other quantities. The module 3DD based on diagonalization of the second-rank CFPs provides the principal values of the second-rank CFPs and the orientation of their principal axis systems w.r.t. the original axis system [3]. The module PAM based on an extension of the cubic/axial pseudosymmetry axes method [4] to monoclinic, orthorhombic (OR), tetragonal I (TEI), and trigonal I (TGI) approximations provides the pseudosymmetry axes that best reflect the approximation to a selected higher symmetry case [5]. This is achieved by minimizing an appropriate combination of the CFPs w.r.t. the Euler angles (α, β, γ), which define the axes determined by the pseudosymmetry axes method. For this purpose the module PAM calculates the 3D surface of the function ε_{sym} w.r.t. the angles α and β as well as the contours of ε_{sym} representing its minima. So obtained CFP sets exhibit the maximal and minimal values of the given higher symmetry CFPs and the out-of-given symmetry ones, respectively. This enables comparison with the experimental CFPs fitted using higher albeit approximated symmetry, e.g. cubic. The closeness factors C_p and the norms ratios R_p provide means for quantitative comparison of various sets of n quantities of the same nature, e.g. the CFPs or the energy levels, considered as n-dimensional (nD) 'vectors' [1,7]. The principal axis systems and pseudosymmetry axes may be compared with the axis systems commonly used in the CF area. For theoretical model calculations, e.g. the ECM ones [2], generally the crystallographic axis system is adopted, which may differ from the rare-earth for a given transition ion. Any experimentally fitted CFPs shall be considered as expressed in an undefined 'nominal' axis system [1]. Comparison and correlation of various axes considered here enable to extract useful structural information, inherent in the low symmetry CFP datasets, and not hitherto utilized. Our three-method approach and analysis of the respective results may facilitate correlation of the optical spectroscopy data with the structural data obtained from X-ray studies. This is

Table 1
The CFP in the extended Stevens notation C_k^q sets (cm^{-1}) and the respective Euler angles (defined in text; in degrees) for Pr^{4+} in $BaPrO_3$: set #1—ECM calculated triclinic set [2], sets #2–#7—after diagonalization of the second-rank CFPs using the module 3DD

α	0	0.433	0.433	90.649	90.649	1.854	1.854
β	0	67.081	67.081	89.490	89.490	157.075	157.075
γ	0	0.553	90.553	−22.920	67.080	91.308	1.308
Si	–	S_1	S_3	S_2	S_5	S_4	S_6

k, q	Set #						
	1	2	3	4	5	6	7
2, 2	130.3	57.2	−57.2	−86.2	86.2	−143.4	143.4
2, 1	123.7	0	0	0	0	0	0
2, 0	3.4	76.5	76.5	−66.9	−66.9	−9.7	−9.7
2, −1	−1.1	0	0	0	0	0	0
2, −2	2.4	0	0	0	0	0	0
$\lambda' = C_2^2/C_2^0$	–	0.747	−0.747	1.289	−1.289	14.831	−14.831
4, 4	−4707.6	3347.1	3347.1	2758.9	2758.9	−4802.1	−4802.1
4, 3	−4183.7	−9566.6	1774.9	1053.8	1014.7	1146.0	3874.6
4, 2	307.4	−4320.5	4320.5	−4656.7	4656.7	−336.1	336.1
4, 1	−3838.5	1885.9	−1340.5	203.2	−1449.1	111.1	3806.1
4, 0	830.3	−329.1	−329.1	−245.1	−245.1	835.0	835.0
4, −1	−341.5	−1340.5	−1885.9	−1449.1	−203.2	−3806.1	111.1
4, −2	60.9	−314.3	314.3	−1920.2	1920.2	−108.6	108.6
4, −3	−1075.4	−1774.9	−9566.6	−1014.7	1053.8	3874.6	−1146.0
4, −4	−1601.9	−46.1	−46.1	2846.0	2846.0	1394.8	1394.8
6, 6	−30.9	820.6	−820.6	254.5	−254.5	45.4	−45.4
6, 5	−2419.0	309.1	850.6	−771.8	543.9	−649.7	2369.7
6, 4	819.0	632.8	632.8	546.4	546.4	882.8	882.8
6, 3	960.0	−361.6	−242.6	−256.9	−391.3	−312.4	−856.0
6, 2	270.2	76.5	−76.5	412.2	−412.2	−275.9	275.9
6, 1	−290.2	−834.2	−150.0	58.8	−103.5	36.6	347.1
6, 0	40.5	−50.9	−50.9	−79.7	−79.7	32.4	32.4
6, −1	−36.8	−150.0	834.2	−103.5	−58.8	−347.1	36.6
6, −2	51.2	−183.7	183.7	183.7	−183.7	41.2	−41.2
6, −3	240.3	242.6	−361.6	391.3	−256.9	−856.0	312.4
6, −4	282.3	22.2	22.2	487.1	487.1	−253.5	−253.5
6, −5	−1062.0	850.6	−309.1	543.9	771.8	−2369.7	−649.7
6, −6	−15.0	124.8	−124.8	726.3	−726.3	−44.7	44.7

evidenced by our consideration of the CFPs for Pr^{4+} in $BaPrO_3$ below.

The original triclinic-like CFPs for Pr1 [2] are listed in Table 1 (set #1). The set #1 yields the rotational invariants [1]: $S_k = 37.28$, 452.00, and 44.48 (cm^{-1}) for $k = 2$, 4, and 6, respectively. All transformed CFP sets in Tables 1–3 yield the same S_k, thus confirming correctness of the respective transformations. The above values of S_4 and S_6 are close to the cubic approximation ones in Refs. [10,11] and for set (1) in Ref. [9], whereas differ from that for set (2) in Ref. [9]; [S_4, S_6] (cm^{-1}) = [447.35, 40.01] and [418.98, 37.65] for Refs. [10,11] [481.39, 55.70] and [283.25, 0.60], for set (1) and (2) in Ref. [9], respectively.

First we determine the principal values of the second-rank CFP 'tensor' and the respective Euler angles (α, β, γ) applying the module 3DD [3] to set #1 in Table 1. The fourth- and sixth-rank CFPs can be transformed accordingly using the CST package [22], so for convenience the transformation expressions have been incorporated into the module 3DD. In Table 1 we provide the six orthorhombic-like sets (#2–#7) corresponding to the original triclinic set #1 for the angles α and β in the range 0–π. The set #2 is chosen as the standard one ($S1$), whereas the remaining sets #3–#7 represent the transformed sets using the orthorhombic standardization transformations Si (S2–S6) defined in Refs. [23,24]. The respective values of the ratio $\lambda' = C_2^2/C_2^0$ are also provided in Table 1. For the orthorhombic-like datasets the ratio λ' describes the 'rhombicity' of the second rank CFPs [23,24], so it is not meaningful in this sense for lower symmetry cases including non-orthorhombic CFPs. In general, the method of diagonalization of the second-rank CFPs yields also other solutions [3], which may alternatively be obtained from the basic ones listed in Table 1 by a rotation 180° around either axis (x, y, z). The resulting sign relationships, noticed also by Burdick et al. [25], are explained in terms of the transformation properties of the CFPs in Ref. [3].

Next we apply the module PAM [5] to set #1 in Table 1 for the angles α and β in the range 0–π. In Table 2 we present the results of the approximation OR, whereas in Table 3 for TEI and TGI. We additionally list the asterisked values $S_k^* = \sqrt{((C_k^0)^2 + (C_k^q)^2/(c_q^k)^2)/(2k+1)}$ for $k = 2, 4$ and 6, based only on the bolded CFPs applicable for a given symmetry approximation used in the pseudosymmetry axes method as well as the asterisked values $\lambda'^* = C_2^2/C_2^0$ defined in Ref. [5].

Table 2
The CFP in the extended Stevens notation C_k^q sets (cm^{-1}) and the respective Euler angles (defined in text; in degrees) for Pr^{4+} in $BaPrO_3$: sets #1–#9 result from the PAM OR approximation

α	4.703	5.036	59.847	50.300	43.111	94.717	146.400	139.121	129.488
β	78.415	168.415	37.468	81.788	126.278	89.935	53.640	98.118	142.423
γ	0.067	0.326	−13.423	−8.202	−10.089	−11.585	−10.218	−8.296	−13.548

k, q	Set #								
	1	2	3	4	5	6	7	8	9
2, 2	**59.9**	**138.7**	**−30.7**	**−19.3**	**−8.3**	**−78.8**	**22.3**	**0.3**	**−2.3**
2, 1	−66.6	66.6	−0.7	−44.9	0.7	3.1	38.6	49.3	−38.6
2, 0	**72.5**	**−6.3**	**4.7**	**−6.7**	**−17.7**	**−66.2**	**−9.0**	**13.0**	**15.6**
2, −1	−39.3	3.1	−231.0	−277.3	−161.3	39.3	164.4	277.3	227.8
2, −2	1.6	19.6	−80.6	24.6	115.5	33.3	113.9	22.4	−82.2
$\lambda'^* = C_2^2/C_2^0$	0.826	−21.935	−6.493	2.900	0.466	1.191	−2.480	0.026	−0.149
4, 4	**3805.7**	**−5192.9**	**3880.2**	**5173.0**	**3902.0**	**3938.3**	**3911.8**	**5167.5**	**3862.2**
4, 3	51.5	−101.4	39.9	−43.7	−39.9	−19.1	51.0	99.3	−50.8
4, 2	**−5217.8**	**−75.7**	**5182.6**	**14.5**	**5170.1**	**−5142.1**	**5162.9**	**11.4**	**5191.3**
4, 1	35.9	14.0	5.7	−6.2	−5.7	−14.1	7.2	14.1	−7.3
4, 0	**−252.1**	**1033.4**	**−255.5**	**1036.2**	**−258.6**	**−271.1**	**−261.6**	**1037.0**	**−254.5**
4, −1	−1.6	5.8	91.8	−37.9	41.9	1.5	−56.0	37.8	−77.7
4, −2	8.3	−3.1	−25.1	−28.4	55.3	21.8	47.0	−12.5	−33.4
4, −3	10.9	39.1	−129.6	265.0	−58.3	−11.0	77.7	−265.1	110.2
4, −4	10.0	0.0	29.3	0.1	−64.2	25.0	−54.3	0.0	39.3
C_4^4/C_4^0	−15.095	−5.025	−15.187	4.992	−15.089	−14.529	−14.955	4.983	−15.176
C_4^2/C_4^0	20.695	−0.073	−20.285	0.014	−19.992	18.970	−19.738	0.011	−20.399
6, 6	**830.9**	**−180.6**	**−822.1**	**−7.0**	**−809.9**	**786.0**	**−806.5**	**−5.5**	**−823.3**
6, 5	−158.6	−101.7	−9.9	−24.3	−29.2	34.3	25.4	47.4	7.4
6, 4	**715.2**	**1185.0**	**730.3**	**−1181.9**	**742.1**	**772.7**	**746.8**	**−1181.3**	**728.0**
6, 3	76.7	41.6	15.5	7.3	2.3	−14.8	0.1	−18.9	−14.9
6, 2	**268.4**	**27.2**	**−349.0**	**−2.8**	**−392.8**	**466.6**	**−403.8**	**−2.8**	**−337.0**
6, 1	−3.4	50.7	0.2	−34.3	6.9	4.0	−7.5	50.5	1.5
6, 0	**−101.0**	**55.6**	**−93.5**	**56.6**	**−89.6**	**−81.8**	**−88.4**	**56.8**	**−94.7**
6, −1	−1.4	12.3	−41.1	−140.4	−14.9	−2.2	11.3	144.0	33.3
6, −2	1.8	0.7	−8.5	10.0	16.7	3.7	14.3	7.1	−9.2
6, −3	5.8	−6.1	−172.8	−86.7	−86.5	3.2	103.5	77.7	159.1
6, −4	−8.4	−3.6	−51.3	5.9	96.5	−47.3	90.2	7.1	−63.8
6, −5	7.3	−11.7	−376.5	−189.9	−195.1	12.5	234.1	170.2	344.6
6, −6	10.2	−0.8	−51.2	60.0	113.5	34.8	99.7	38.6	−54.5
C_6^6/C_6^0	−8.226	−3.250	8.789	−0.123	9.038	−9.604	9.120	−0.096	8.695
C_6^4/C_6^0	−7.081	21.325	−7.807	−20.880	−8.282	−9.442	−8.445	−20.802	−7.689
C_6^2/C_6^0	−2.657	0.490	3.731	−0.050	4.383	−5.701	4.567	−0.050	3.559
S_2^*/S_2 (%)	96.32	96.32	22.00	15.56	22.00	96.32	18.83	15.56	18.83
S_4^*/S_4 (%)	100.00	100.00	99.99	99.99	99.99	100.00	99.99	99.99	99.99
S_6^*/S_6 (%)	99.91	99.91	99.35	99.32	99.35	99.91	99.39	99.32	99.39

Comparison of the two types, i.e. total and asterisked, of (i) the rotational invariants and (ii) the 'rhombicity' ratio for the second rank CFPs provides a measure of the goodness of the given higher symmetry approximation. Comparison of the OR results, which represent both the four- and two-fold pseudosymmetry axes, with the TEI ones, which represent only the four-fold pseudosymmetry axes, enables recognition of the OR solutions that correspond to the four-fold pseudosymmetry axes, whereas the remaining solutions, i.e. not assigned in this way, correspond to the two-fold ones. The results in Tables 2 and 3 indicate the following correspondence between the OR and TEI solutions: OR#2 and TEI#1, OR#4 and TEI#2, OR#8 and TEI#3. This is confirmed by the respective closeness factors C_p and the norms ratios R_p for the respective H_{CF} terms: $k = 2, 4, 6$, and the global (gl) ones. We obtain C_2, C_4, C_6, and C_{gl} equal nearly exactly 1.0 (within the eight decimal places) for each pair of the OR and TEI sets, whereas all R_p equal exactly 1.0. The solutions for the TGI approximation represent the three-fold pseudosymmetry axes. However, the TGI approximation can be considered only as following directly from the triclinic CFP case, without the ascent of symmetry via the monoclinic, orthorhombic, and tetragonal approximation. This shows the greater usefulness of the latter approximations over the former one. The difference in the orientation of the respective z-axes being the four-fold (three-fold) pseudosymmetry axis for the approximation TEI (TGI) is illustrated in Fig. 1.

Table 3
The CFP C_k^q sets (cm^{-1}) and the respective Euler angles (defined in text; in degrees) for Pr^{4+} in $BaPrO_3$ after the TEI approximation (sets #1–#3) and TGI approximation (sets #4–#7); ES—the extended Stevens and NS—the normalized Stevens notation

α	5.039	5.039	50.300	50.300	139.121	139.121	4.647	4.746	102.806	86.641
β	168.413	168.413	81.788	81.788	98.118	98.118	43.148	113.679	55.490	124.379
γ	0.328	0.328	−8.202	−8.202	−8.295	−8.295	0.096	0.072	−14.106	−14.084

k, q	Set #									
	1 (ES)	1′ (NS)	2 (ES)	2′ (NS)	3 (ES)	3′ (NS)	4 (ES)	5 (ES)	6 (ES)	7 (ES)
2, 2	138.7	80.1	−19.3	−11.1	0.3	0.2	70.4	101.8	−98.0	−99.5
2, 1	66.6	19.2	−44.9	−13.0	49.3	14.2	126.4	−170.8	−111.8	113.9
2, 0	**−6.3**	**−6.3**	**−6.7**	**−6.7**	**13.0**	**13.0**	**61.9**	**30.5**	**−47.0**	**−45.5**
2, −1	3.1	0.9	−277.3	−80.1	277.3	80.1	−33.9	−30.3	−6.4	70.5
2, −2	19.6	11.3	24.6	14.2	22.4	13.0	−10.1	12.6	38.5	15.8
$\lambda' * = C_2^2/C_2^0$	−21.932	–	2.900	–	0.026	–	1.138	3.335	2.088	2.188
4, 4	**−5192.9**	**−877.8**	**5173.0**	**874.4**	**5167.5**	**873.5**	−53.4	−85.0	42.3	54.7
4, 3	−101.0	−6.0	−43.7	−2.6	99.3	5.9	**−19398.5**	**19488.3**	**−19627.5**	**19592.5**
4, 2	−75.7	−16.9	14.5	3.3	11.4	2.6	−5.1	−0.7	−18.7	−20.6
4, 1	14.5	2.3	−6.2	−1.0	14.1	2.2	35.0	−67.2	−61.9	74.3
4, 0	**1033.4**	**1033.4**	**1036.2**	**1036.2**	**1037.0**	**1037.0**	**−703.3**	**−694.3**	**−680.2**	**−683.7**
4, −1	5.6	0.9	−37.8	−6.0	37.7	6.0	−9.0	12.5	−29.7	26.2
4, −2	−3.1	−0.7	−28.4	−6.3	−12.5	−2.8	−0.8	4.0	6.2	1.4
4, −3	39.3	2.3	265.1	15.8	−265.2	−15.8	0.0	0.0	0.0	0.0
4, −4	0.0	0.0	0.0	0.0	0.0	0.0	12.9	8.6	25.2	29.5
C_4^4/C_4^0	−5.025	–	4.992	–	4.983	–	–	–	–	–
C_4^3/C_4^0	–	–	–	–	–	–	27.581	−28.071	28.856	−28.656
6, 6	−180.6	−16.8	−7.0	−0.6	−5.5	−0.5	**923.6**	**950.2**	**993.9**	**987.1**
6, 5	−101.4	−2.7	−24.3	−0.7	47.4	1.3	−217.7	431.7	336.9	−374.3
6, 4	**1185.0**	**149.3**	**−1181.9**	**−148.9**	**−1181.3**	**−148.8**	−48.4	−91.1	58.0	65.2
6, 3	41.5	2.9	7.2	0.5	−18.9	−1.3	**−1425.3**	**1293.4**	**−1104.4**	**1132.9**
6, 2	27.2	3.8	−2.8	−0.4	−2.8	−0.4	−28.2	−39.8	36.5	41.7
6, 1	50.7	5.5	−34.3	−3.7	50.5	5.5	−40.4	47.6	35.4	−41.6
6, 0	**55.6**	**55.6**	**56.6**	**56.6**	**56.8**	**56.8**	**92.5**	**98.0**	**105.5**	**104.4**
6, −1	12.3	1.3	−140.4	−15.3	144.0	15.7	6.7	−0.6	27.4	−23.0
6, −2	0.7	0.1	10.0	1.4	7.1	1.0	−4.5	−2.9	−20.0	−16.9
6, −3	−6.1	−0.4	−86.7	−6.0	77.8	5.4	−2.7	−1.6	4.8	−7.0
6, −4	−3.6	−0.5	5.9	0.7	7.1	0.9	6.4	7.6	26.9	30.4
6, −5	−11.8	−0.3	−190.0	−5.1	170.2	4.6	−28.9	40.5	−157.9	160.7
6, −6	−0.8	−0.1	60.0	5.6	38.6	3.6	3.2	−1.5	−6.5	−11.9
C_6^4/C_6^0	21.325	–	−20.879	–	−20.802	–	–	–	–	–
S_2^*/S_2 (%)	7.59	7.59	7.99	7.99	15.56	15.56	74.28	36.61	56.33	54.56
S_4^*/S_4 (%)	99.99	99.99	99.99	99.99	99.99	99.99	100.00	99.99	99.99	99.99
S_6^*/S_6 (%)	99.33	99.33	99.33	99.33	99.33	99.33	99.80	99.37	99.57	99.48

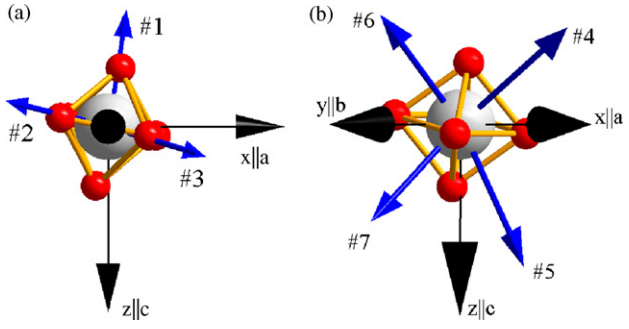

Fig. 1. The z-axis obtained using the module PAM for each of the three solutions in the TEI (a) and the four solutions in the TGI approximation (b).

In order to extract useful structural information inherent in the respective Euler angles sets and the CFPs sets in Tables 2 and 3, we need to carry out theoretical analysis of the transformation properties of CF Hamiltonian in Eqs. (3) and (4) and then analyze correspondingly the original CFPs and the axis systems used [2,12]. The authors [2] have implicitly adopted the crystallographic axis system defined in Fig. 1 of Rosov et al. [12], in which the Pr-ligands complex (see Fig. 1 of Ref. [6]) has the orientation corresponding to the 45°/Oz rotation discussed in Section 2. Note that the axes x and y directed towards ligands represent the so-called first-kind orthorhombic symmetry, whereas the 45°/Oz rotation represents the so-called second-kind orthorhombic symmetry [26]. Correspondingly, for cubic symmetry, the former axis system, which applies to H_{CF} in Eq. (3), may be defined as the basic cubic axis system, whereas the

latter axis system, which applies to H_{CF} in Eq. (4), as the 45°/Oz rotated cubic axis system. The two axis systems yield the cubic CFP ratios (C_4^4/C_4^0, C_6^4/C_6^0) as (5, −21) and (−5, 21), respectively. Transformations of H_{CF} in Eq. (3) using any orthorhombic transformation S2 to S6 [23,24] leave H_{CF} invariant and thus preserve the CFP ratios. This invariance, however, does not apply fully to H_{CF} in Eq. (4). Only the transformation S3 leaves H_{CF} invariant, whereas other transformations, resulting in the change of the z-axis to a two-fold axis, yield H_{CF} in the form:

$$H_{CF} = \{C_4^0\}\beta(-\tfrac{1}{4}O_4^0 \pm 5O_4^2 + \tfrac{15}{4}O_4^4) + \{C_6^0\}\gamma(-\tfrac{13}{8}O_6^0 \mp \tfrac{105}{16}O_6^2 + \tfrac{105}{8}O_6^4 \mp \tfrac{231}{16}O_6^6) \quad (5)$$

where the curly brackets denote the original CFPs, whereas the upper sign applies to S2 and S4, while the lower sign to S5 and S6. The transformed CFPs denoted by the square brackets result from Eq. (5) as $C_k^q \equiv \text{const}\{C_k^q\}$. The CFPs $[C_4^2]$, $[C_6^2]$, and $[C_6^6]$ reflect the apparent orthorhombic symmetry for the purely cubic H_{CF} expressed in the transformed axis systems. Eq. (5) yields the following relations for the transformed cubic CFPs (S2 and S4—upper sign; S5 and S6—lower sign): $[C_4^4/C_4^0] = -15$, $[C_4^2/C_4^0] = \mp 20$, $[C_6^6/C_6^0] = \pm 231/26 \approx \pm 8.88$, $[C_6^4/C_6^0] = -105/13 \approx -8.08$, and $[C_6^2/C_6^0] = \pm 105/26 \approx \pm 4.04$. In a similar way in Ref. [21] we have considered the S2 to S6 transformations and derived the relations for the second-rank CFPs for tetragonal I and II symmetry as well as both kinds of orthorhombic symmetry. The general relations [21] are used below to analyze the TEI and OR approximations within the pseudosymmetry axes method.

Analysis of the TEI and OR sets in view of the theoretical relations derived above enable the following observations. The TEI sets #2 and #3 in Table 3 correspond to the basic cubic axis system, whereas the set #1 corresponds to the 45°/Oz rotated cubic axis system. Due to the correspondence discussed above, the same applies to the equivalent OR sets (#2, #4, and #8). The z-axes for the sets #1–#3 are mutually perpendicular to each other, whereas the orientations of the x- and y-axes vary. Importantly, the calculated ratios C_4^4/C_4^0 and C_6^4/C_6^0 for sets #1–#3 in Table 3 turn out to be very close to the theoretical ones for pure cubic symmetry in Eqs. (3) and (4). This reveals the very high degree of cubic symmetry of the fourth- and sixth-rank CFPs in TEI sets #1–#3. The calculated CFP ratios for the remaining OR sets #1, #3, #5–#7, and #9 yield also the values closely corresponding to the cubic ones, so in this case those arising from H_{CF} in Eq. (5). The second-rank ratios calculated for (i) the basic cubic axis system: $\lambda'^* = C_2^2/C_2^0$ (TEI#2: ≈ 3 and TEI#3: ≈ 0) and (ii) the 45°/Oz rotated cubic axis system: $\lambda'^* = C_2^{-2}/C_2^0$ (TEI#1: ≈ 3) are very close to the theoretical values as indicated. In both cases these ratios indicate that the Pr^{4+} site symmetry is very close to tetragonal, whereas the small values of the respective CFPs reveal symmetry very close to cubic. Hence, overall the results from the pseudosymmetry axes method, both in the TEI and OR approximation, indicate that the local site symmetry of Pr^{4+} ion is close to cubic with a slight triclinic distortion. This agrees well with the hypothesis put forward by Bickel et al. [9]. Additionally, for the basic cubic axis system, where the fourfold rotation axes are chosen as the quantization axes, the positive signs of C_4^0 and C_4^4 indicate that the symmetry at the Pr^{4+} site is very close to the cubic octahedral (six-fold coordination) one. Note that the negative sign of C_4^0 and C_4^4 would indicate [27] the cubic tetrahedral (four-fold coordination) or the regular cube (eight-fold coordination).

Analysis of the TGI approximation also confirms the above conclusion that the local site symmetry of Pr^{4+} ion is close to cubic with a slight triclinic distortion. In the trigonal axes taken along one of the three-fold axis and one two-fold axis, the calculated ratio of the cubic CFPs: $C_4^3/C_4^0 \approx \pm 28$ is very close to the theoretical value indicated.

In Table 3 we list also the CFPs in the normalized Stevens (NS) notation [14,17,18] for selected sets to illustrate the apparently different relative strength of the CFPs expressed in the two notations. It turns out that the cubic character of the fourth- and sixth-rank CFPs, which is accounted for by specific parameter ratios, is more directly evident if we consider C_k^q(NS) instead of C_k^q in the extended Stevens notation. Interestingly, the TEI set #1 (as well as #2 and #3) turns out to be very close to the cubic CFPs for Pr^{4+} in $BaCeO_3$ [10] (cm^{-1}): $C_4^0 = 1025$, $C_6^0 = 51$, $C_4^4 = -5125\,(5125)$, and $C_6^4 = 1071\,(-1071)$. The dominant cubic fourth-rank CFPs and relatively small non-cubic ones suggest that fourth-rank CFPs may have been reliably determined in Ref. [2]. However, for the sixth-rank CFPs, although the cubic CFP C_6^4 is dominant, C_6^0 in the extended Stevens notation is smaller than some non-cubic sixth-rank CFPs. Conversion to the normalized Stevens notation yields as dominant C_4^0(NS), C_4^4(NS), C_6^0(NS), and C_6^4(NS). Thus C_k^q(NS) in Table 3 reveal considerably different parameter ratios. Overall the relative CFP values may suggest either more pronounced low symmetry effects for the sixth-rank CFPs or, most probably, their less accurate determination in Ref. [2]. Hence, it turns out that the normalized Stevens notation provides more accurate representation of the relative strength of the CFPs, whereas the extended Stevens notation yields apparently misleading CFP ratios. This is due to the different multiplication factors implicit in the q-components in the two notations. Importantly, the normalized Stevens operators are 'normalized' in the quantum mechanical sense, namely, the product of their transformation matrices is equal to 1 (for details, see Ref. [17]). Hence, C_k^q(NS) enable more meaningful assessment of the relative strength of CFPs.

A word of caution is pertinent here concerning two aspects (A) and (B) bearing on the triclinic-like nature of any theoretical CFP sets and their reliability. (A) Generally, the smaller number of the non-zero CFPs, the higher local site symmetry. However, the great number of the non-zero CFPs (even maximum of 27 required for $4f^N$ ions at triclinic sites) does not necessarily mean that the local site symmetry around an impurity ion is triclinic. Our considerations [19] reveal that an apparently low symmetry CFP set may indicate the choice of an axis system that does not coincide with the appropriate rare-earth. In order to verify which symmetry case actually applies, one needs to consider in details the crystallographic data, if available, and determine the appropriate rare-earth. A partial indication of the actual local site symmetry may be obtained by analysis of the observed degeneracy of the energy levels, since complete or partial removal of

degeneracy may indicate lower symmetry, e.g. triclinic or monoclinic. **(*B*)** It appears that the triclinic distortion is most evident in the second-rank CFPs (original set #1 in Table 1), which remain highly triclinic in the TEI approximation (sets #1–#3 in Table 3). This may represent the actual low symmetry effects inherent in the second-rank CFPs. However, it cannot be excluded that the low symmetry effects observed in the CFPs [2] are due to some computational artifacts. Our recent ECM calculations for Cr^{3+} ion in Cs_2NaAlF_6 [19] and Ni^{2+} ion in $MgAl_2O_4$ [28] yielded the initial CFPs exhibiting local site symmetry lower than the expected D_{3d}. The choice of the surrounding ions is crucial to ensure that the cluster preserves properly the RE^{3+} site symmetry. Avoiding the artificial effects due to corners, edges, and/or missing ions may not be an easy matter for large clusters. In fact, any finite truncation of the crystal lattice within the ECM cluster calculations may yield CFPs of apparently lower symmetry than applicable. Appearance of some non-zero CFPs may be due to computational artifacts, which may originate from either some rounding-off errors or inclusion/exclusion in the lattice summations of some distant ions that overall do not preserve the site symmetry. This may also apply to the CFPs [2] since the authors suspect improper estimations of their C_2^q based on the observation that some calculated energy levels differ significantly from the measured ones. To split the degenerate cubic energy levels some non-cubic CFPs are necessary, however, any improper estimations of CFPs [2] may yield the second-rank CFPs exhibiting apparent low symmetry. The most pronounced low symmetry effects may be due to the second-rank non-axial CFPs, which should be responsible for the observed splitting of the energy levels Γ_8 and Γ_8' [2] indicating axial or lower symmetry. We note that the orthorhombic CFPs C_2^2 and C_2^0 (sets #2 and #3 in Table 3) are very small as compared with the remaining lower symmetry CFPs C_2^1, C_2^{-1}, and C_2^{-2}. If not the large non-zero values of the latter CFPs, this would indicate the case very close to cubic symmetry. This discrepancy may suggest that the CFPs C_2^2 and C_2^0 calculated using the ECM [2] are accurate, however, doubts arise concerning the CFPs C_2^1, C_2^{-1}, and C_2^{-2}. Our experience [19,28] indicates that the energy levels discrepancies [2] are most likely due to the computational artifacts discussed above. Hence, a careful re-check of the ECM calculations [2] would be useful in order to obtain a more reliable and symmetry-consistent CFP set.

In analogy with the EMR data, it may be expected that the principal axis system of the second-rank CFPs may be somewhat correlated with the principal axes of the theoretical g-factor and tensor A_{ij} [2]. Concerning the principal axes of the tensor A_{ij} Popova et al. [2] have only mentioned that these axes are slightly turned away from the axes of the g-tensor (angles of rotations are less than 10°). The principal values of the g-tensor of the ground doublet for the Pr1 site were calculated [2] as −0.6827, −0.7295 and −0.8369. The corresponding principal axis system of the g-factor in the crystallographic axis system [2] were expressed in terms of the unit vectors: $\mathbf{u_1}$ (0.0531, −0.9928, 0.1075), $\mathbf{u_2}$ (−0.5288, 0.0634, 0.8464), and $\mathbf{u_3}$ (0.8471, 0.1018, 0.5216). The module 3DD enables us also to calculate the respective unit vectors in the crystallographic axis system for all set being solutions of diagonalization of the second-rank CFPs as well as all solutions obtained using the module PAM in each approximation defined above. We have adhered to the r.h.s. convention for the axes. It turns out that the unit vector for set #2 (3DD) in Table 1 is very close, except for the orientation, to the unit vector for the g-tensor [2], namely, $u_x' = -u_2$, $u_y' = -u_1$, and $u_z' = -u_3$, whereas the principal values are rearranged as follows: $g_x = -0.7295$, $g_y = -0.6827$, and $g_z = -0.8369$. Concerning the pseudosymmetry axes method results, only the OR approximation yields one solution (#1 in Table 2), with the x-axis parallel to the four-fold axis and the y- and z-axes parallel to the two-fold axis, which is most close to the principal axis system of the second-rank CFPs as well as to the unit vectors of the g-tensor calculated by us based on data [2]. The principal axis system of the second-rank CFPs (3DD), sets #2, #4, and #7 in Table 1, are very close to the principal axis system obtained in the OR approximation (#1, #6 and #2 in Table 2), respectively. The latter sets correspond to the 45°/Oz rotated orthorhombic axes. For comparison, the orientation of the respective axes: (i) principal axis system of the g-factor [2], (ii) principal axis system of the second-rank CFPs (3DD) for set #2 in Table 1, and (iii) OR approximation fourth-rank CFPs for set #1 in Table 2 is presented in Fig. 2.

The closeness factors and the norms ratios have been calculated between pairs of various quantities: (i) the cubic fourth- and sixth-rank CFPs and the respective global quantities obtained by us in the TEI approximation (Table 3) and those taken from literature sources (Table 4), (ii) the energy level sets for Pr^{4+} ions in $BaPrO_3$ (and $BaCeO_3$) in triclinic and/or cubic symmetry approximation (Table 5), and (iii) the experimental [12,29] structural parameters (Pr–O bonds and O–Pr–O angels) at various temperatures listed in Table 6. The latter quantities are overall very close as reflected by the closeness factors and the norms ratios: $C_p \in 0.999971$–0.99999993 and $R_p \in 0.995$–0.99976. Hence we refrain from providing the respective table. For the CFPs in Table 3 the closeness factors and the norms ratios listed in Table 4 confirm that the CFPs cal-

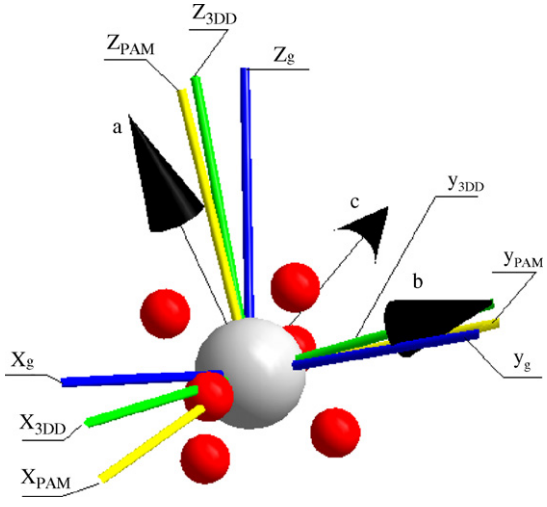

Fig. 2. The principal axes (x_i, y_i, z_i) for the g-tensor, the 3DD principal values of the second-rank CFPs (set #2 in Table 1), and the fourth-rank CFPs in the PAM OR approximation (set #1 in Table 2).

Table 4
The closeness factors C_p and the norms ratios R_p for the cubic fourth- and sixth-rank CFPs and the respective global quantities between the pairs (i, j) of various CFP sets: the triclinic CFPs obtained in the PAM TEI approximation—sets #1–#3 (cubic CFPs only in Table 3), sets #5 and #6 [9], set #7 [10], and set #4 [11]

Pair/quantity	(1, 4)	(1, 5)	(1, 6)	(1, 7)	(6, 7)
C_4	1.00000	1.00000	1.00000	1.00000	1.00000
C_6	1.00000	1.00000	1.00000	1.00000	1.00000
C_{gl}	0.99996	0.99977	0.99346	0.99995	0.99454
R_4	0.8592	0.8813	0.3929	0.9799	0.4009
R_6	0.7264	0.6292	0.0002	0.8200	0.0002
R_{gl}	0.8574	0.8765	0.3875	0.9777	0.3964
Pair/quantity	(4, 5)	(4, 6)	(4, 7)	(5, 6)	(5, 7)
C_4	1.00000	1.00000	1.00000	1.00000	1.00000
C_6	1.00000	1.00000	1.00000	1.00000	1.00000
C_{gl}	0.99953	0.99448	1.00000	0.99082	0.99952
R_4	0.7573	0.4572	0.8769	0.3462	0.8636
R_6	0.4571	0.0003	0.8858	0.0001	0.5160
R_{gl}	0.7516	0.4520	0.8770	0.3397	0.8570

Note that sets #2 and #3 yields the same values as set #1 in pairs with other sets #4–#7.

Table 5
The closeness factors C and the norms ratios R between pairs (i, j) for the energy level sets E_i: E_1–E_3 and E_6 are the sets listed in Table 1 of Ref. [2] denoted by the cubic irreps Γ_i; E_1 ($T = 120$ K) and E_2 ($T = 16$ K)—experimental values, E_3—ECM calculated, E_6—quoted from [10], whereas E_4 (E_5)—calculated set 1 (alternative set 2) of Table 2 in Ref. [9]

Pair/quantity	(E_1, E_2)	(E_1, E_3)	(E_1, E_4)	(E_1, E_5)	(E_1, E_6)
C	0.9999982	0.9999529	0.9998600	0.9969977	0.9999877
R	0.9944116	0.9784687	0.9081661	0.7487859	0.9538995
Pair/quantity	(E_2, E_3)	(E_2, E_4)	(E_2, E_5)	(E_2, E_6)	(E_5, E_6)
C	0.9998731	0.9998680	0.9968968	0.9998337	0.9978140
R	0.9942829	0.9264945	0.6951086	0.9849529	0.6846492
Pair/quantity	(E_3, E_5)	(E_3, E_6)	(E_3, E_6)	(E_4, E_6)	(E_4, E_6)
C	0.9999118	0.9974016	0.9999523	0.9969726	0.9998567
R	0.9211976	0.6991054	0.9793218	0.6440142	0.9406485

Note that seven energy levels are taken into account for all sets, except for set E_1 comprising six energy levels.

culated based on the ECM reflect very closely cubic symmetry. The following correlations may be noted. For each sets #1–#3 (TE) in Table 3 compared with a given literature set using only the cubic CFPs we obtain the values of C_p and R_p ($p = 4$, 6, gl): (i) very close for set #7 taken from Ref. [10]—the ranges: $C_p \in 0.99995$–1.00000 and $R_p \in 0.8200$–0.9799, (ii) quite close for set #4 (#5) of Ref. [11] ([9]): $C_p \in 0.99977$–1.00000 and $R_p \in 0.6292$–0.8813. For set #6 (the alternative CFP set obtained in Ref. [9]) compared with sets #1–3, the closeness factors are very close: $C_p \in 0.99346$–1.00000, however, the norms ratios show disparity: $R_p \in 0.0002$–0.3929, thus confirming that the set #6 is physically unacceptable [9]. The closeness factors and the norms ratios listed in Table 5 indicate that all energy level sets for Pr^{4+} in $BaPrO_3$ at triclinic and/or cubic symmetry approximation, namely, E_1, E_2 and E_3 (Table 1 of Ref. [2]), E_4—the calculated set 1 of Table 2 [9], and E_6 for Pr^{4+} in $BaCeO_3$ [10], are mutually very close ($C_p \in 0.9998600/0.9999982$ and $R_p \in 0.9081661/0.9944116$).

Table 6
Comparison of the structural parameters for the Pr–O_6 complex in $BaPrO_3$: the Pr–O bonds (in pm) and the O–Pr–O angles (°)

	Set # (temperature (K))					
	1 (300) [12]	2 (17) [12]	3 (5) [12]	4 (16) [29]	5 (2) [29]	6 (–) [11]
Pr–O2	222.33	223.05	223.35	223.46	223.15	222 ± 3
Pr–O2	222.27	221.97	221.66	222.29	222.40	
Pr–O1	222.52	222.87	222.78	223.08	223.15	223 ± 6
O1–Pr–O2	90.342	89.837	89.860	89.713	89.435	
O1–Pr–O2	90.528	90.568	90.778	91.204	91.283	
O2–Pr–O2	88.414	88.342	88.317	88.228	88.260	

For E_5, i.e. the set 2 of Table 2 [9] calculated using the alternative CFP set [9], we obtain very close $C_p \in 0.9968968/0.9978140$, while disparate $R_p \in 0.6440142/0.7487859$, thus reinforcing the above conclusion concerning the alternative CFP set #6 of Ref. [9]. The closeness factors and the norms ratios in Tables 4 and 5 enable quantitative correlations of various sets of comparable quantities.

4. Summary and conclusions

This paper provides framework for comprehensive analysis of crystal field parameter (CFP) datasets for transition ions at low symmetry sites, which enables extracting useful structural information. As a case study, the full results of analysis of the triclinic-like CFP [2] dataset as well as the cubic ones obtained by various authors for Pr^{4+} ion in $BaPrO_3$ are presented, whereas the preliminary results were presented in the conference paper [6]. Our investigations concern several aspects, which are briefly summarized as follows.

The method of diagonalization of the second-rank CFPs, and the standardization idea involved therein, have been extended to triclinic symmetry. Our literature survey indicates that several authors still lack awareness of the orthorhombic and monoclinic standardization, which have been proposed in the 1985s. Thus incompatible CFP datasets, i.e. with the fitted or calculated 'rhombicity' ratio lying in various ranges, do appear in the literature. The major point is that the large non-standard values of this ratio do not indicate large orthorhombic distortions in crystals and hence such data may lead to physically wrong conclusions. For meaningful comparisons of CFPs the datasets must be first transformed into the same nominal axis system w.r.t. both the orientation of axes and their direction, to ensure that the 'rhombicity' ratio is in the standard range. Thus the standard range is strongly recommended for the CFP presentation.

The pseudosymmetry axis method has been extended from tetragonal and trigonal type II symmetry to monoclinic, orthorhombic, tetragonal and trigonal type I symmetry. We have developed a computer module PAM with the major features: graphical visualization capabilities; determination of the Euler angles (α, β, γ) that define the pseudosymmetry axes, which have structural interpretation; accordingly transformed CFPs of the rank $k = 2, 4, 6$. The orthorhombic and axial approximations have been applied to the fourth- and sixth-rank triclinic-like CFPs for Pr^{4+} in $BaPrO_3$. Comparison of the results from the pseudosymmetry axes method for various approximations enables extracting useful structural information. The closeness factors and the norms ratios, which have recently been introduced to facilitate quantitative comparison of CFP datasets as well as the energy level sets, have also been calculated.

Major findings arising from the calculations, using the method of diagonalization of the second-rank CFPs, the pseudosymmetry axis method, and the closeness factors and norms ratios, for the cubic and triclinic-like CFPs for Pr^{4+} in $BaPrO_3$ are as follows: (i) the results arising from the first method show that the strength of low symmetry effects inherent in the second-rank CFPs appear quite large, whereas the large discrepancy between S_2^* (original triclinic CFPs: $q = 0, 2$) and S_2 (total obtained also from the module 3DD) indicates significant deviation of the crystallographic axis system from the principal axis system of the second-rank CF terms, (ii) the method of diagonalization of the second-rank CFPs is equivalent to Burdick and Reid [30] method, however, but their method for the fourth- and sixth-rank CFPs has no clear not physical sense, (iii) the orthorhombic approximation within the pseudosymmetry axes method visualizes fourfold and twofold pseudo-symmetry axes determined w.r.t. the crystallographic axis system, whereas the tetragonal (trigonal) approximation visualizes the three (four) equivalent four- (three-) fold pseudosymmetry axes and (iv) the structural model of site symmetry arising from the calculations using the module PAM shows that in spite of the buckling of the $Pr–O_6$ octahedra the local site symmetry of the complex is very close to cubic octahedral one.

Additional advantages of the comprehensive approach reside in the fact that both the method of diagonalization of the second-rank CFPs and the pseudosymmetry axis method yield several physically equivalent CFP sets. Thus these CFP sets may be used in the multiple correlated fitting technique for additional fittings using such CFP sets as starting values. This would yield several correlated datasets. Finding the intercorrelations between these sets requires knowledge of the transformation properties of CFPs. This need enhances the role of the package CST for conversions, standardization, transformations of crystal field (zero-field splitting) parameters. The multiple correlated fitting technique offers ways to increase accuracy and reliability of final fitted CFPs, identify global minima, and eliminate spurious sets (computational artifacts).

In summary, the comprehensive approach proposed here comprising three methods outlined above, together with the multiple correlated fitting technique, proved to be useful in optical studies of low symmetry systems. Application of the three-method approach to the triclinic-like CFPs for Pr^{4+} ion in $BaPrO_3$ [2] confirms the usefulness of our comprehensive approach. The axes determined using the method of diagonalization of the second-rank CFPs and the pseudosymmetry axes method have been related to the structural data. The principal axes of the second-rank CFPs obtained due to the former method have been correlated with the principal axes of the g-factor and the A-tensor determined in Ref. [2]. The apparent low symmetry nature of the triclinic-like CFPs [2] determined in the crystallographic axis system [12] becomes evident due to application of the pseudosymmetry axes method extended to orthorhombic and axial cases. Thus the hypothesis concerning the cooperative buckling of Pr-octahedra reducing the local site symmetry, while preserving the nearly octahedral geometry for the Pr site [2] is supported by our considerations.

Importantly, our approach may help experimentalists to better interpret and analyze optical data as well as to extract useful structural information from CFP datasets for transition ions at low symmetry sites. This approach appears timely, whereas other applications of this approach for rare-earth ions in various hosts and reanalysis of the CFP as well as zero-field splitting parameter datasets for several other ion-host systems will be considered elsewhere.

Acknowledgements

This work was partially supported by the research grant from the Polish Ministry of Science and Tertiary Education in the years 2006–2009. P. Gnutek acknowledges gratefully the opportunity of PhD program (under the CZR supervision) at the Institute of Physics, SUT.

References

[1] C. Rudowicz, J. Qin, J. Lumin. 110 (2004) 39.
[2] M.N. Popova, S.A. Klimin, L.A. Kasatkina, G. Cao, J. Crow, Phys. Lett. A 223 (1996) 308.
[3] C. Rudowicz, P. Gnutek, in preparation.
[4] G. Bacquet, J. Dugas, C. Escribe, J.M. Gaite, J. Michoulier, J. Phys. C 7 (1974) 1551.
[5] C. Rudowicz, P. Gnutek, J. Mag. Reson., submitted for publication.
[6] C. Rudowicz, P. Gnutek, J. Alloys Compd., in press.
[7] C. Rudowicz, P. Gnutek, M. Karbowiak, Phys. Rev. B, submitted for publication.
[8] M.N. Popova, S.A. Klimin, S.A. Golubchik, G. Cao, J. Crow, Phys. Lett. A 211 (1996) 242.
[9] M. Bickel, G.L. Goodman, L. Soderholm, B. Kanellakopulos, J. Solid State Chem. 76 (1988) 178.
[10] Y. Hinatsu, N. Edelstein, J. Solid State Chem. 112 (1994) 53.
[11] S. Kern, C.-K. Loong, G.H. Lander, Phys. Rev. B 32 (1985) 3051.
[12] N. Rosov, J.W. Lynn, Q. Lin, G. Cao, J.W. O'Reilly, P. Pernambuco-Wise, J.E. Crow, Phys. Rev. B 45 (1992) 982.
[13] B.Z. Malkin, in: A.A. Kaplyanskii, R.M. Macfarlane (Eds.), Spectroscopy of Solids containing Rare-earth Ions, North-Holland, Amsterdam, 1987, p. 13.
[14] C. Rudowicz, Magn. Res. Rev. 13 (1987) 1;
C. Rudowicz, Magn. Res. Rev. 13 (1988) 335.
[15] C. Rudowicz, S.K. Misra, Appl. Spectrosc. Rev. 36 (2001) 11.
[16] A. Abragam, B. Bleaney, Electron Paramagnetic Resonance of Transition Ions, Clarendon Press, Oxford, 1970.
[17] C. Rudowicz, J. Phys. C 18 (1985) 1415;
C. Rudowicz, J. Phys. C 18 (1985) 3837.
[18] C. Rudowicz, C.Y. Chung, J. Phys.: Condens. Matter 16 (2004) 5825.
[19] C. Rudowicz, M.G. Brik, N.M. Avram, Y.Y. Yeung, P. Gnutek, J. Phys.: Condens. Matter 18 (2006) 5221.
[20] C. Rudowicz, Chem. Phys. 97 (1985) 43.
[21] C. Rudowicz, P. Gnutek, G.W. Burdick, in preparation.
[22] C. Rudowicz, Computer package CST conversions, standardization and transformations, in: D.J. Newman, B. Ng (Eds.), Crystal Field Handbook, vol. 259, Cambridge Univ. Press, 2000.
[23] C. Rudowicz, R. Bramley, J. Chem. Phys. 83 (1985) 5192.
[24] C. Rudowicz, J. Chem. Phys. 84 (1986) 5045.
[25] G.W. Burdick, S.M. Crooks, M.F. Reid, Phys. Rev. B 59 (1999) R7789.
[26] C. Rudowicz, J. Phys. Chem. Solids 38 (1977) 1243.
[27] C. Görller-Walrand, K. Binnemans, in: K.A. Gschneidner Jr., L.R. Eyring (Eds.), Handbook on the Physics and Chemistry of Rare Earths, vol. 23, Elsevier, Amsterdam, 1996, p. 121.
[28] M.G. Brik, N.M. Avram, C.N. Avram, C. Rudowicz, Y.Y. Yeung, P. Gnutek, J. Alloys Compd. 432 (2007) 61.
[29] D.J. Goosens, R.A. Robinson, M.T.F. Telling, Physica B 352 (2004) 105.
[30] G.W. Burdick, M.F. Reid, Mol. Phys. 102 (2004) 1141.